PCCP

Accepted Manuscript

This is an *Accepted Manuscript*, which has been through the Royal Society of Chemistry peer review process and has been accepted for publication.

Accepted Manuscripts are published online shortly after acceptance, before technical editing, formatting and proof reading. Using this free service, authors can make their results available to the community, in citable form, before we publish the edited article. We will replace this *Accepted Manuscript* with the edited and formatted *Advance Article* as soon as it is available.

You can find more information about *Accepted Manuscripts* in the Information for Authors.

Please note that technical editing may introduce minor changes to the text and/or graphics, which may alter content. The journal's standard Terms & Conditions and the Ethical guidelines still apply. In no event shall the Royal Society of Chemistry be held responsible for any errors or omissions in this *Accepted Manuscript* or any consequences arising from the use of any information it contains.

ROYAL SOCIETY OF CHEMISTRY

www.rsc.org/pccp

Surface hopping investigation of benzophenone excited state dynamics

Lucilla Favero[†], Giovanni Granucci[‡] and Maurizio Persico[‡]

[†] *Università di Pisa, Dipartimento di Farmacia via Bonanno Pisano 33, 56126 Pisa, Italy*

[‡] *Università di Pisa, Dipartimento di Chimica e Chimica Industriale, via Moruzzi 13, 56124 Pisa, Italy*

Abstract

We present a simulation of the photodynamics of benzophenone for the first 20 ps after $n \rightarrow \pi^*$ excitation, performed by trajectory surface hopping calculations with on the fly semiempirical determination of the potential energy surfaces and electronic wavefunctions. Both the dynamic and the spin-orbit couplings are taken into account, and the time-resolved fluorescence emission is also simulated. The computed decay time of the S_1 state is in agreement with experimental observations [13, 14]. The direct $S_1 \rightarrow T_1$ InterSystem Crossing (ISC) accounts for about 2/3 of the S_1 decay rate. The remaining 1/3 goes through T_2 or higher triplets. The nonadiabatic transitions within the triplet manifold are much faster than the ISC and keep the population of T_1 at about 3/4 of the total triplet population, and that of the others states (mainly T_2) at 1/4. Two internal coordinates are vibrationally active immediately after $n \rightarrow \pi^*$ excitation: one is the C=O stretching and the other one is a combination of the conrotatory torsion of the phenyl rings and of the bending involving the carbonyl C atom. The period of the torsion-bending mode coincides with oscillations in the time-resolved photoelectron spectra of Spighi et al [14] and substantially confirms their assignment.

Keywords: Benzophenone - Nonadiabatic dynamics - InterSystem Crossing - Surface Hopping - Spin-orbit coupling

1 Introduction

The photoexcited benzophenone chromophore shows an efficient intersystem crossing (ISC), relaxing to the triplet states with a quantum yield close to 1 [1]. For this reason it is widely used in photochemistry as a triplet sensitizer [2], and may induce DNA damage [3, 4]. It is moreover commonly used as UV blocker [5]. Benzophenone derivatives have been proposed [6] as constituents of organic light emitting diodes (OLEDs) and, thanks to their high photoluminescence quantum yield and large Stokes shift, could be good candidates for the the design of organic luminescent solar concentrators [7] (LSCs).

The $S_1(n \rightarrow \pi^*)$ state of benzophenone gives rise to a broad and weak absorption band, with λ_{max} at about 345 nm in gas phase [8], corresponding to an excitation energy $\Delta E_{exc} = 3.6$ eV. The mechanism of ISC from S_1 to T_1 after $n \rightarrow \pi^*$ excitation is still a matter of debate, particularly concerning the role of higher lying triplet states. Shah et al. [9] performed transient absorption experiments on benzophenone in solution (acetonitrile) with $\Delta E_{exc} = 4.64$ and 3.70 eV, corresponding respectively to excitation in the $\pi \rightarrow \pi^*$ and in the upper energy end of the $n \rightarrow \pi^*$ band. In both cases a lifetime for the $S_1 \rightarrow T_1$ ISC of ~ 10 ps is obtained by fitting the rise of the transient absorption signal at 530 nm, which roughly corresponds to the λ_{max} of T_1. This is in agreement with older results obtained in acetonitrile, benzene and ethanol [10–12] while a slightly larger ISC lifetime of 16–18 ps was reported in isooctane [11, 12].

The $S_1 \rightarrow T_1$ decay of benzophenone in solution was thoroughly reinvestigated by Aloïse et al. [13] with transient absorption experiments considering various solvents and excitation energies. After excitation in the lower energy end of the $n \rightarrow \pi^*$ band ($\Delta E_{exc} = 3.24$ eV), the transient signals at 570 and 525 nm, corresponding respectively to the λ_{max} of S_1 and T_1, were fitted. In acetonitrile they obtained a lifetime for the S_1 decay of 17 ps, while the increase of the T_1 signal gave 9.4 ps. Slightly longer times were obtained for the T_1 growth in methanol and CH_2Cl_2 (11.6 and 11.8 ps, respectively). With $\Delta E_{exc} = 4.64$ eV in acetonitrile, roughly the same lifetime of ~ 10 ps was obtained for the decay of S_1 (but fitting the transient absorption at 330 nm) and the growth of T_1. These raw data were further mathematically analyzed, and a two step kinetic model was found $S_1 \rightarrow IS \rightarrow T_1$, were *IS* is an intermediate state, not fully identified. The characteristic times for the transitions $S_1 \rightarrow IS$ and $IS \rightarrow T_1$ were reported to be ~ 6 ps and ~ 10 ps respectively, largely independent of the solvent and of the excitation energy.

Very recently Spighi et al. [14] performed time resolved photoelectron spectroscopy experiments for benzophenone in a supersonic jet and deposited on cold argon clusters, with $\Delta E_{exc} = 4.66$ eV. The time constants for the $S_1 \rightarrow T_1$ ISC were found to depend on the environment: 5 ps for the free molecule and 20 ps for deposited benzophenone. This has been interpreted as a signature of the presence of a threshold energy to reach the S_1/T_1 intersection from the S_1 minimum. Strong oscillations with a period of 550 fs in the decay of the photoelectron intensity were observed, and attributed to the totalsymmetric ring torsional motion in S_1.

In the present work we investigate the photodynamics of isolated benzophenone after $n \rightarrow \pi^*$ excitation by nonadiabatic molecular dynamics simulations, in the framework of the surface hopping method [15]. The spin orbit interaction is included and evaluated on the fly during the dynamics, so that both internal conversion (IC) and ISC processes can be accounted for in our simulations [16–18]. Our aim is to clarify the mechanism of the $S_1 \rightarrow T_1$ decay, in particular concerning the role of higher lying triplet states.

2 Potential energy surfaces

The electronic potential energy surfaces (PES) and couplings considered in the nonadiabatic dynamics calculations have been obtained using a semiempirical reparameterized AM1 Hamiltonian, with the Floating Occupation Molecular Orbitals Configurations Interaction (FOMO-CI) ansatz [15]. In particular, the CI subspace selected comprised 76 determinants, and was generated from an active space of 10 MO and 10 electrons, considering first a full CI of 6 MO and 10 electrons and then adding the single excitations (generated from the doubly occupation determinant) involving the remaining 4 virtual orbitals. Three of the active MOs belonged to the carbonyl group (the highest non-bonding MO n_{O} plus π_{CO} and π^*_{CO}), and seven to the phenyl rings (three bonding MOs, π_{ring} and four antibonding, π^*_{ring}). A Gaussian width for floating occupation of 0.1 Hartree was chosen.

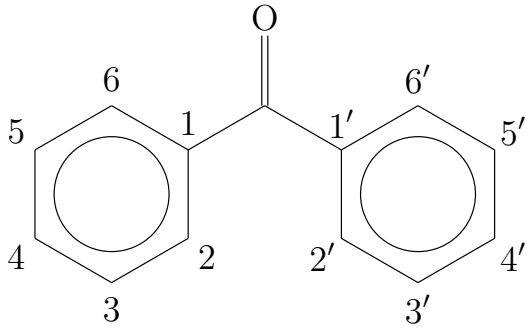

Figure 1: Benzophenone. The numbering of phenyl carbon atoms is shown.

The improved set of semiempirical parameters was obtained by minimizing the quadratic errors with respect to given target values, according to the procedure fully described in ref. [19]. Mainly experimental data were used as targets, as shown in Table S1 of Supporting Information. The new semiempirical parameters for carbon, hydrogen and oxygen issued from the fit are shown in Table S2. Note that two different set of parameters were produced for carbonylic and aromatic carbon atoms. Our reparameterization was per-

Table 1: Equilibrium geometries. Distances in Å, angles in degrees. θ is the angle between the planes of the phenyl rings [20]. For C_2 geometries the distances C-C_1 and C-$C_{1'}$ share the same value, as well as the angles C_1CO and $C_{1'}CO$, and the dihedrals OCC_1C_2 and $OCC_{1'}C_{2'}$

	S_0	S_1	S_2	T_1	T_2
C-O	1.23	1.33	1.25	1.31	1.26
C-C_1/C-$C_{1'}$	1.45	1.41	1.45/1.42	1.42	1.41/1.45
$C_1CC_{1'}$	121	133	121	131	124
$C_1CO/C_{1'}CO$	120	114	119/120	114	119/117
θ	51	37	41	40	53
$OCC_1C_2/OCC_{1'}C_{2'}$	-150	-159	-168/-140	-157	-134/-170

formed before we became aware of the recent high level ab initio calculations of Sergentu et al. [21], reporting vertical excitation energies at CASPT2(16/15) level and minimum energy paths on S_1, S_2, T_1 and T_2.

The most relevant geometrical parameters of benzophenone ground and lower lying states minima are shown in Table 1 (see Figure 1 for the numbering of atoms). The S_1 and T_1 minima share the same C_2 conformation as the ground state with, as expected, significant but relatively small geometrical changes, mainly concerning the C-O bond length and the rotation of the phenyl rings around the C-C_1 and C-$C_{1'}$ bonds. Such rotation takes place in the conrotatory mode, which is more effective than the disrotatory one in relieving the repulsion between the H atoms in 2 and 2′ with a minimal loss of conjugation of the carbonyl and phenyl π systems. For this reason we shall use a single parameter to describe the phenyl rotation, namely the dihedral angle θ between the two phenyl planes (see note [20] for details). The variations in the geometrical parameters upon excitation are in reasonable agreement with the CASSCF results of Sergentu et al. [21]. The T_2 minimum correspond to a T_1/T_2 intersection.

In Table 2 we show vertical and adiabatic excitation energies (ΔE_{vert} and ΔE_{adia}), comparing our semiempirical FOMO-CI results to available experimental and computational data. Figure 2 offers a schematic view of the relationships between minima and surface crossings. The experimental adiabatic $S_0 \rightarrow S_1$ and $S_0 \rightarrow T_1$ transition energies are accurately reproduced, as well as the absorption, fluorescence and phosphorescence maxima that can be identified with ΔE_{vert} computed at the S_0, S_1 and T_1 minima, respectively. $\Delta E_{vert}(S_0 \rightarrow S_n)$ and $\Delta E_{vert}(S_0 \rightarrow T_n)$ are also in good agreement (within 0.13 eV) with the CASPT2(16/15) results of Sergentu et al. [21], at least for S_1 and T_1-T_3. The agreement deteriorates for higher lying states, still remaining reasonable. Rather large differences are also found between the semiempirical and the ab initio $\Delta E_{vert}(S_1 \rightarrow S_0)$ and $\Delta E_{vert}(T_1 \rightarrow S_0)$, i.e. for the luminescence bands, but in this case our results are closer to the experimental ones.

In Table 2 we also show vertical transition energies obtained from our state averaged CASSCF(16/13), which includes 16 states (6 singlets and 10 triplets), and was performed with the 6-31G* basis set at the B3LYP/6-31G* ground state minimum. If compared to the available experimental data, and to the CASPT2 results of ref. [21], the CASSCF transition energies are invariably too high, providing therefore a much worse description of benzophenone PES's with respect to FOMO-CI.

Minimum energy conical intersections (MXS) between S_0/S_1 and S_0/T_1 were determined at the FOMO-CI level. For S_0/S_1 two distinct, highly distorted, MXS structures were found (enolic and cyclopropanone, see Figure 2), at 4.38 and 4.04 eV above the ground state minimum, respectively. The presence of the enolic S_0/S_1 MXS was subsequently confirmed by ab initio state averaged CASSCF(16/13) calculations including S_0, S_1 and T_1, performed using the 6-31G* basis set and the MOLPRO program package [22], which located the MXS at 4.20 eV above the S_0 minimum, in good agreement with the semiempirical result. Analogously, a cyclopropanone S_0/S_1 MXS was obtained with CASSCF, at 4.32 eV above the S_0 minimum. An enolic MXS was also found for S_0/T_1, at 3.52 eV above the ground state minimum according to FOMO-CI. These distorted MXS lie around or higher than the S_1 Franck-Condon energy, indicating that fast $S_1 \rightarrow S_0$ or $T_1 \rightarrow S_0$ deactivation pathways are not readily accessible by $n \rightarrow \pi^*$ excitation.

The S_1/T_1 MXS is found at 0.45 eV above the S_1 minimum, with a planar geometry. The energies of S_1 and T_2 at the S_1 minimum are, respectively, 3.30 and 3.55 eV while at the T_2 minimum they are 3.55 and 3.32, so that the two states must cross proceeding

from one minimum to the other. In fact, the S_1/T_2 MXS is found at an intermediate geometry with respect to S_1 and T_2 equilibrium points shown in table 1, and only 0.09 eV above the S_1 minimum. Note moreover that T_2 and S_1 are almost degenerate in the Franck-Condon region (see table 2). Overall, the above pattern for S_1 and T_2 closely match the ab initio results of Sergentu et al. (see in particular the T_2 minimum energy path shown in figure 7 of Ref. [21]).

The spin orbit (SO) interaction among FOMO-CI semiempirical wavefunctions was evaluated using a mean field Hamiltonian fully described elsewhere [23]. The relevant SO semiempirical parameters for carbon and oxygen were fitted in order to reproduce ab initio CASSCF results. In particular, the target SO couplings were obtained from

Table 2: Vertical and adiabatic transition energies, in eV. Values used as targets in the reparameterization are given in bold. C_2 symmetry labels are indicated were appropriate. The T_1/T_2 MXS (minimum energy intersection) corresponds to the minimum of the T_2 PES, according to our FOMO-CI calculations.

Transition	FOMO-CI[a]	CASSCF[a]	CASPT2 [21]	Exp
ΔE_{adia}				
$S_0(A)_{min} \rightarrow S_1(A)_{min}$	3.30		3.15	**3.25**[b]
$S_0(A)_{min} \rightarrow T_1(A)_{min}$	3.09		2.85	**3.00**[b]
$S_0(A)_{min} \rightarrow T_1/T_2$ MXS	3.32		3.22	
ΔE_{vert} (absorption)				
$S_0(A)_{min} \rightarrow S_1(A)$	3.53	4.46	3.66	**3.61**[c]
$S_0(A)_{min} \rightarrow S_2(A)$	4.56	5.60	4.33	**4.40**[d]
$S_0(A)_{min} \rightarrow S_3(B)$	4.57	5.62	4.43	**4.40**[d]
$S_0(A)_{min} \rightarrow S_4(B)$	4.76	6.00	5.39	**5.00**[e]
$S_0(A)_{min} \rightarrow S_5(A)$	5.05	6.64		**5.00**[e]
$S_0(A)_{min} \rightarrow T_1(A)$	3.26	3.88	3.33	
$S_0(A)_{min} \rightarrow T_2(A)$	3.51	4.25	3.41	
$S_0(A)_{min} \rightarrow T_3(B)$	3.57	4.32	3.69	
$S_0(A)_{min} \rightarrow T_4(A)$	3.85	5.05	4.18	
$S_0(A)_{min} \rightarrow T_5(B)$	3.86	5.17	4.18	
$S_0(A)_{min} \rightarrow T_6(A)$	4.07	5.19	4.22	
$S_0(A)_{min} \rightarrow T_7(B)$	4.11	5.27	4.26	
$S_0(A)_{min} \rightarrow T_8(A)$	4.92	6.90		
$S_0(A)_{min} \rightarrow T_9(B)$	4.93	6.65	6.47	
ΔE_{vert} (emission)				
$S_1(A)_{min} \rightarrow S_0(A)$	2.93		2.34	**2.95**[f]
$T_1(A)_{min} \rightarrow S_0(A)$	2.84		2.19	**2.78**[c]-2.72[f]

[a]This work. [b]Supersonic jet, 0-0 band [25–27]. [c]Absorption/phosphorescence, band maximum, low pressure vapor [8]. [d]Absorption, band shoulder, solution [28, 29]. [e]Absorption, band maximum, solution [28, 29]. [f]Fluorescence/phosphorescence, band maximum, solution [30].

Table 3: Spin orbit coupling, cm^{-1}. For geometry specifications see the text.

coupling	geometry	CASSCF	FOMO-CI
S_0/T_1	planar	57	62
S_1/T_2	planar	41	38
T_1/T_2	planar	55	52
S_0/T_1	perp	61	63
S_0/T_2	perp	0.02	0.13
S_1/T_1	perp	0.03	0.09
S_1/T_2	perp	34	25
T_1/T_2	perp	46	33

state averaged CASSCF(16/13)/6-31G* calculations including 16 states. In agreement with Sergentu et al. [21] the T_1 state showed non negligible $n \rightarrow \pi^*/\pi \rightarrow \pi^*$ mixing, the extent of which is influenced by the value of the angle θ between the phenyl rings: for planar geometries ($\theta = 0°$) $n \rightarrow \pi^*$ and $\pi \rightarrow \pi^*$ configurations belong to different irreducible representations, so that no mixing is possible. Therefore, according to El-Sayed rules [24], the SO coupling between T_1 and $S_1(n \rightarrow \pi^*)$ is in turn influenced by the angle θ (see figure 3). To avoid inconsistencies due to differences in $n \rightarrow \pi^*/\pi \rightarrow \pi^*$ mixing with FOMO-CI wavefunctions with respect to CASSCF, the target SO couplings were determined at geometries where the mixing is zero for symmetry reasons: the planar C_{2v} ($\theta = 0°$) geometry and the perpendicular C_s ($\theta = 90°$) geometry, obtained minimizing

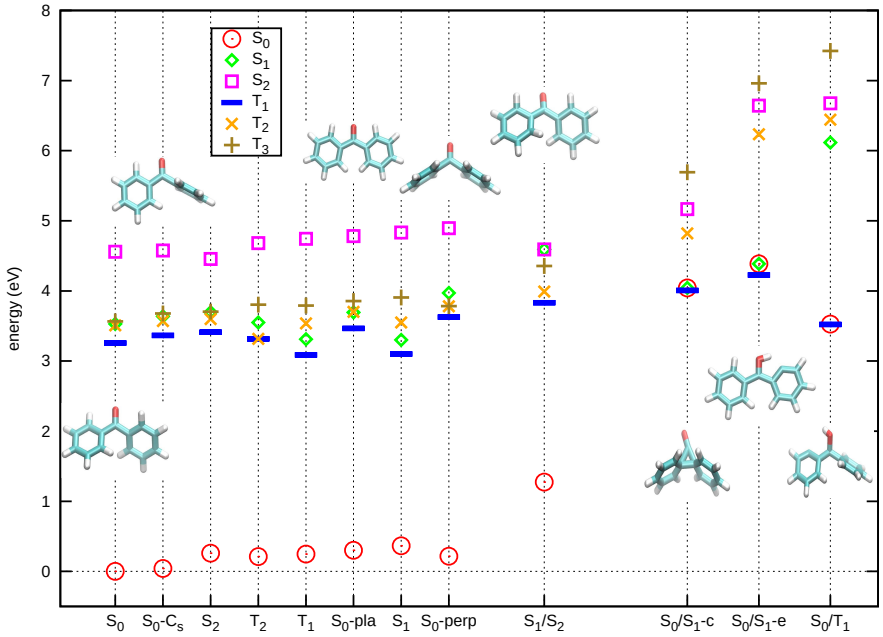

Figure 2: Potential energy surfaces of benzophenone: schematic view of minimum energy points. Labels S_0/S_1-e and S_0/S_1-c refer respectively to enolic and cyclopropanone minimum energy conical intersections.

the S_0 energy with respect to the other internal coordinates. In this way the semiempirical SO parameters for C and O were evaluated, respectively, as $\xi_C = 28.6$ cm^{-1} and $\xi_O = 222$ cm^{-1}. In table 3 we show the target CASSCF SO couplings and the corresponding FOMO-CI results at the planar and perpendicular geometries referred above. In the following, we shall refer to the SO coupling strength, computed as the square root of the sum of the squares of the multiplet components. The dependence of the S_1/T_1 and S_1/T_2 SO coupling on the orientation of the phenyl planes is shown in figure 3. As one can see from table 3, with the fitted semiempirical SO parameters the FOMO-CI wavefunctions reproduce well the ab initio results. At the ground state equilibrium geometry the semiempirical S_1/T_1 and S_1/T_2 SO couplings are, respectively, 6 and 26 cm^{-1}, to be compared with the CASSCF values of 20 and 29 cm^{-1}. Given the good results of table 3, the discrepancy in the S_1/T_1 SO coupling at the ground state minimum has to be attributed to the different $n \rightarrow \pi^*/\pi \rightarrow \pi^*$ mixing in the semiempirical wavefunctions with respect to CASSCF.

3 Excited state dynamics

The nonadiabatic molecular dynamics calculations have been performed with our surface hopping scheme [15], using the spin-adiabatic method [16] to account for the SO interaction. In particular, we selected the first 6 singlet and 10 triplet states giving rise to 36 spin-adiabatic (i.e. spin-mixed) states after diagonalization of the SO Hamiltonian. In all the dynamics calculations the PESs and couplings were obtained on the fly with the FOMO-CI method and the semiempirical parameters referred above. To sample the starting conditions a ground state trajectory was run for 100 ps, with an integration time step of 0.1 fs, using the Bussi Parrinello algorithm [31] to introduce the coupling with a thermostat at 298 K.

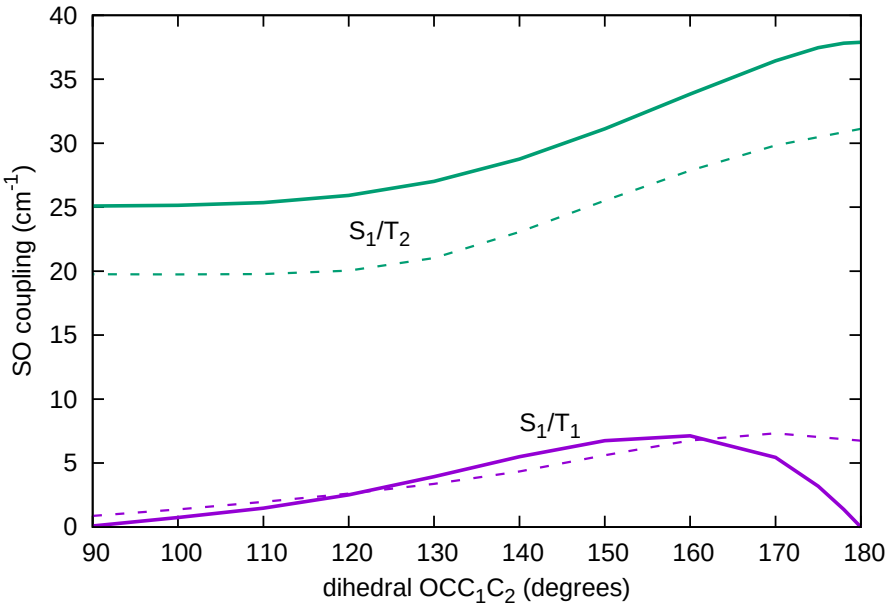

Figure 3: S_1/T_1 and S_1/T_2 spin orbit coupling (cm^{-1}) with respect the OCC_1C_2 dihedral. Solid (respectively, dashed) lines: the $OCC_{1'}C_{2'}$ dihedral is kept fixed at 180° (respectively, 150°). All the other internal coordinates are optimized for the ground state.

In the present work, excitation in the $n \rightarrow \pi^*$ band is considered: the starting conditions were therefore selected from the thermalized trajectory (discarding the first 20 ps) in agreement with the radiative transition probability to the spin-adiabatic states in the energy range 3.35–3.75 eV, following a stochastic algorithm described elsewhere [15]. Overall, 320 starting conditions were selected and the corresponding surface hopping trajectories were propagated for 20 ps. A single trajectory was discarded for technical reasons, so that the final averages shown here are obtained from a total of 319 trajectories. An integration time step of 0.1 fs was used both for the nuclear and for the electronic degrees of freedom. In particular, for the latter ones the local diabatization scheme was employed [32,33]. The quantum decoherence was approximately taken into account using our overlap based correction [34] with Gaussian width $\sigma = 0.2$ a.u. and overlap threshold $S_{min} = 0.005$.

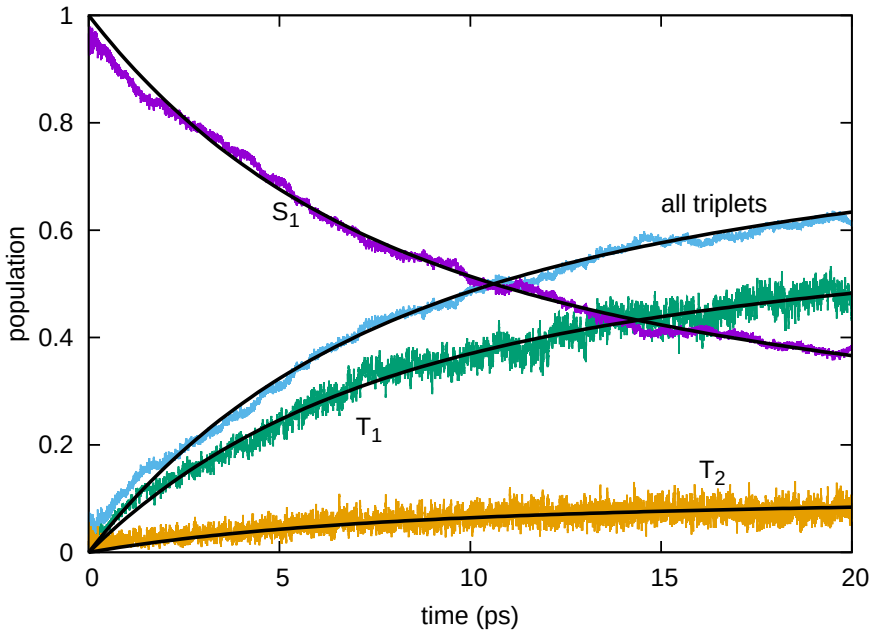

Figure 4: Spin-diabatic state populations after $n \rightarrow \pi^*$ excitation. Black curves are biexponential fits of the state populations. Only states with final population larger than 5% are shown.

As the SO coupling in benzophenone is weak, the results are better analyzed in terms of the spin-diabatic (i.e. unmixed) singlet and triplet states. In figure 4 we show the time evolution of the spin-diabatic state populations:

$$\overline{P}_K(t) = N_{traj}^{-1} \sum_j \sum_m |\langle K_m | A^{(j)}(t) \rangle|^2 \quad (1)$$

Here N_{traj} is the total number of trajectories, the index j runs over all trajectories, the index m identifies the components of the spin multiplet K, and $A^{(j)}(t)$ is the current spin-adiabatic state for the trajectory j at time t [17, 18]. The fit of $\overline{P}_{S_1}(t)$ with an exponential function $e^{-t/\tau}$ yielded $\tau = 16.2$ ps. This result is in good agreement with the lifetime of 17 ps obtained by Aloïse et al. [13] in their experiments with $\Delta E_{exc} = 3.24$ eV in acetonitrile, by a monoexponential fit of their raw transient absorption data. A more refined representation for the decay of the S_1 population is obtained by fitting $\overline{P}_{S_1}(t)$ with a biexponential function

$$\overline{P}_{S_1}(t) = we^{-t/\tau_1} + (1-w)e^{-t/\tau_2} \quad (2)$$

Table 4: Radiationless transition rates $\overline{R}_{KL}$ (ps^{-1}) and rate constants $\overline{T}_{KL}$ between spin-diabatic states (or groups of states), averaged over time intervals $[t_1, t_2]$ (ps).

state K	state(s) L	t_1, t_2	$\overline{R}_{K\to L}$	$\overline{R}_{L\to K}$	$\Delta\overline{R}_{K\to L}$	$\overline{T}_{K\to L}$	$\overline{T}_{L\to K}$
S_1	T_1	0, 5	0.038	0.005	0.033	0.045	0.051
S_1	T_1	5,10	0.036	0.007	0.029	0.061	0.022
S_1	T_1	10,15	0.027	0.012	0.015	0.058	0.029
S_1	T_1	15,20	0.015	0.014	0.001	0.038	0.030
S_1	T_1	0,20	0.029	0.009	0.019	0.051	0.033
S_1	$T_2 - T_{10}$	0, 5	0.115	0.093	0.022	0.139	1.376
S_1	$T_2 - T_{10}$	5,10	0.093	0.085	0.009	0.160	1.421
S_1	$T_2 - T_{10}$	10,15	0.085	0.084	0.001	0.185	1.341
S_1	$T_2 - T_{10}$	15,20	0.083	0.076	0.006	0.210	1.042
S_1	$T_2 - T_{10}$	0,20	0.094	0.085	0.010	0.174	1.295
T_1	$T_2 - T_{10}$	0, 5	1.453	1.468	-0.015	10.057	25.446
T_1	$T_2 - T_{10}$	5,10	3.525	3.523	0.002	11.207	44.560
T_1	$T_2 - T_{10}$	10,15	4.798	4.794	0.004	11.773	83.343
T_1	$T_2 - T_{10}$	15,20	5.238	5.241	-0.003	11.348	82.707
T_1	$T_2 - T_{10}$	0,20	3.753	3.756	-0.003	11.096	59.014

In this case we get $\tau_1 = 6$ ps, $\tau_2 = 53$ ps and $w = 0.49$. Although the biexponential function fits our data much better than the single exponential, it is clear that this value of τ_2 is only a rough estimate, because it largely exceeds the duration of our simulation. The τ_1 value is close to the lifetime of 5 ps observed in time-resolved photoelectron spectra of the isolated molecule after $\pi \to \pi^*$ excitation by Spighi et al [14], who assigned it to the ISC decay of S_1.

During 20 ps only 2 trajectories out of 319 undergo $S_1 \to S_0$ decay, which is not enough for a meaningful statistics. It is however clear that the internal conversion rate of S_1 must be negligible in this time scale, so that the lifetime of S_1 is practically determined by the ISC process. In the same time interval, no trajectories switch from the triplet states to S_0. Therefore, within the first tens of picoseconds we expect the rise of the total triplet population to be almost exactly complementary to the decay of S_1, i.e.

$$\overline{P}_{\mathrm{all-triplets}}(t) = 1 - \overline{P}_{S_1}(t) \tag{3}$$

as shown in figure 4. The population of every single triplet increases almost exactly with the same law, being at all times a fraction of the total: about 76% T_1, 13% T_2, 4% T_3, and 6% T_4 together with the higher triplets, of which the last with a non negligible contribution is T_8 (see figures 4, S1 and S2). Overall, the population of triplets other than T_1 is considerable and can significantly contribute to probe signals such as differential absorption or photoionization, because of the different spectral properties of these states (we remind that T_1 is essentially $n \to \pi^*$, while T_2, T_3 and most of the others are $\pi \to \pi^*$).

To analyze in more detail the nonadiabatic dynamics we monitored the switches between quasi-diabatic states (or multiplets). A $K \to L$ switch for trajectory j is counted

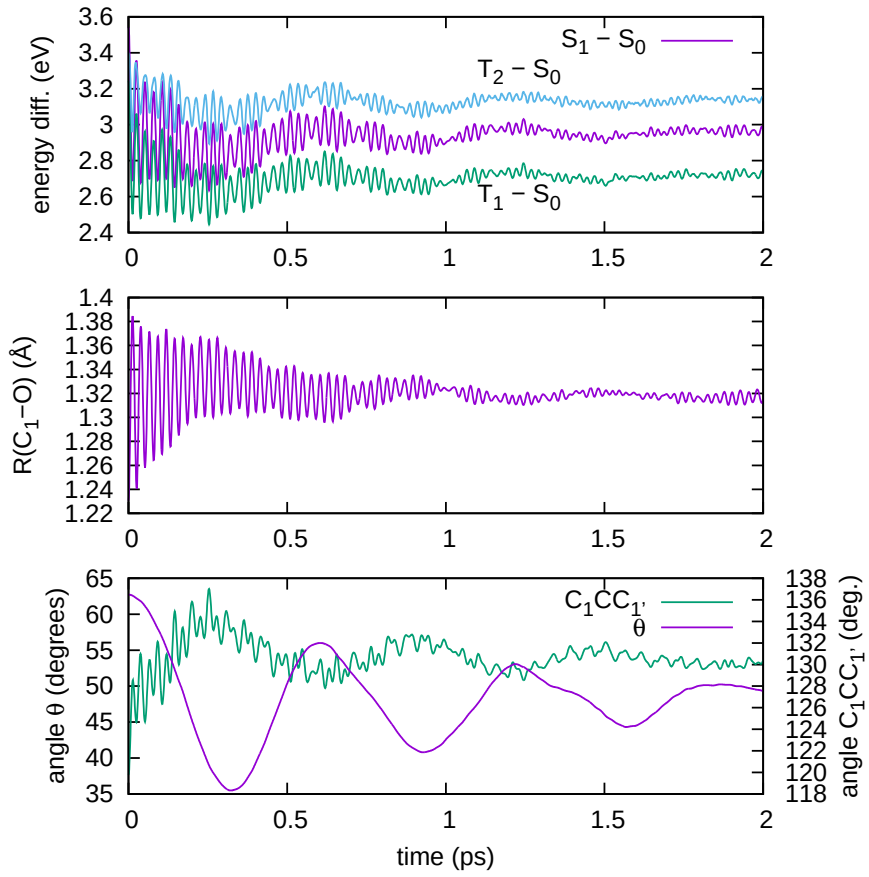

Figure 5: Energetic and geometrical variables, averaged over the full swarm of trajectories, in the 0–2 ps time domain. Upper panel: energy differences $E(S_1) - E(S_0)$, $E(T_1) - E(S_0)$ and $E(T_2) - E(S_0)$, in eV. Middle panel: distance C-O, in Å. Lower panel: angles θ and $C_1CC_{1'}$, in degrees. Note the scale for $C_1CC_{1'}$ on the right side.

when K is replaced by L as the multiplet K with the largest probability $P_K^{(j)}(t) = \sum_m |\langle K_m | A^{(j)}(t) \rangle|^2$ (see ref. [18] for details). We calculate the one-way transition rate $\overline{R}_{K\to L}(t_1, t_2)$ between states K and L, averaged over all trajectories, on the basis of the number $N_{K\to L}(t_1, t_2)$ of $K \to L$ switches occurring in the time interval $[t_1, t_2]$:

$$\overline{R}_{K\to L}(t_1, t_2) = \frac{N_{K\to L}(t_1, t_2)}{N_{traj}\ (t_2 - t_1)} \tag{4}$$

In a similar way, we define the corresponding rate constant

$$\overline{T}_{K\to L}(t_1, t_2) = N_{traj}^{-1}\ (t_2 - t_1)^{-1} \sum_i \left[\overline{P}_K(t_i)\right]^{-1} \tag{5}$$

Here the index i runs over all the $K \to L$ switches occurring at times $t_i \in [t_1, t_2]$. We qualify $\overline{T}_{K\to L}$ as a "rate constant" because the $1/\overline{P}_K(t_i)$ factor is meant to normalize the transition rate with respect to the population of the starting state; but of course

$\overline{T}_{K\to L}$ is determined by the dynamics and may change in time. In table 4 we list the one-way rates and rate constants for different time intervals, along with the net rates $\Delta\overline{R}_{K\to L} = \overline{R}_{K\to L} - \overline{R}_{L\to K}$. For simplicity, we group together all the triplets from T_2 to T_{10}, but in table S3 we provide more detailed data. Some of the rate constant values cannot be determined with a good statistical accuracy, because they depend on a small number of switches and/or on small state probabilities $\overline{P}_K$: quite understandably, this occurs at short times ($[0, 5]$ ps time interval) for triplet $\to$ singlet transitions. Apart from such uncertainties, the rate constants do not show dramatic changes, probably because the geometrical relaxation and the internal vibrational energy redistribution occur in a shorter time scale and/or their effect on the transition rates is minor.

The $S_1 \rightleftarrows T_2$ ISC rates exceed the $S_1 \rightleftarrows T_1$ ones in both directions, because of the larger spin-orbit coupling and smaller energy gap for the former transition. However, the forward and backward $S_1 \rightleftarrows T_2$ rates tend to cancel out, so the net contribution of the T_2 route to the decay of S_1 is smaller than that of T_1: overall, during the first 20 ps the $S_1 \to T_1$ net rate is about twice the sum of the net rates from S_1 to T_2 and all the higher triplets. The ISC net transition rates tend to slow down as the S_1 population decreases, showing a tendency towards equilibrium. Much faster exchanges, but again with relatively small net effects on the state populations, are caused by the dynamic couplings within the triplet manifold. This can be appreciated from the noisy character of the T_1 and T_2 curves in figure 4, if compared to S_1 and the total triplet populations. Overall, some population from T_2 and the higher triplets leaks to T_1, especially during the first picoseconds, but the population flux seems to follow the circular route $T_1 \to T_2 \to$ higher triplets $\to T_1$.

The internal coordinates most affected by the $n \to \pi^*$ excitation are the R_{CO} distance, the $CC_1C_{1'}$ angle and the θ dihedral (see Table 1). In both S_1 and T_1 the carbonyl group acquires an extra π electron and the stabilizing effect of conjugation with the phenyl groups becomes more important than in the ground state. As a consequence, the phenyl groups tend to rotate towards planarity (smaller θ) and the $C_1CC_{1'}$ angle opens to relieve the repulsion between H_2 and $H_{2'}$. In figure 5 we present the time evolution of some energetic and geometrical variables, averaged on the full swarm of trajectories, in the 0–2 ps domain, when S_1 is by far the most populated state. The averaged energy differences $E(X) - E(S_0)$, with $X = S_1$, T_1 or T_2, show fast oscillations with the same period of the C-O stretch, further modulated by the oscillations of θ. Differently with respect to the Franck-Condon point, the T_2 curve lies sensibly higher in energy with respect to S_1: this can be understood considering that the minimum energy geometry of T_2 is quite different from that of S_1 and T_1 (see table 1). $C_1CC_{1'}$ and θ oscillate with the same period but with opposite phases, in agreement with the above considerations. In addition, $C_1CC_{1'}$ is clearly affected by the C=O stretching motion. The period of the combined θ and $C_1CC_{1'}$ mode is about 600 fs, which is in nice agreement with the oscillation period of 550 fs observed for the time resolved photoelectron intensity in the experiments of Spighi et al. [14]. Therefore, we substantially confirm their attribution of this feature to the ring torsional motion in S_1.

The evaluation of the transition dipole moments along the nuclear trajectories allows us to simulate the decay of the fluorescence intensity [35]. The photon emission rate averaged over all the trajectories is shown in figure 6. The spikes that represent sudden increases in the emission rate, in particular around 13 ps, are due to transitions to S_2. The $\pi \to \pi^*$ states have a much larger oscillator strength with respect to S_1, so that a very modest population of the S_2 state (below 1%) can lead to a sizeable increase in the emission rate. In fact, very few trajectories do switch to S_2, which means this contribution

to the emission rate, besides being of secondary importance, cannot be accurately assessed on the basis of our simulation.

We fitted the emission rate with the exponential function

$$F(t) = K_F e^{-t/\tau_F} \tag{6}$$

and we obtained the fluorescence rate constant $K_F = 0.23\ \mu s^{-1}$ and the lifetime $\tau_F = 17.5$ ps. As almost the whole emission originates from S_1, τ_F is close to the lifetime obtained by a monoexponential fit of the S_1 population. Also the fluorescence rate shows evidence of a more complex decay, that can be approximated by a biexponential law:

$$F(t) = K_F[we^{-t/\tau_1} + (1-w)e^{-t/\tau_2}] \tag{7}$$

However, it was not possible to obtain reliable values of the four parameters K_F, w, τ_1 and τ_2 from the fitting procedure, so we assumed $\tau_1 = 6$ ps and $\tau_2 = 53$ ps as for the S_1 population. Then, the fitting yielded $K_F = 0.25\ \mu s^{-1}$ and $w = 0.52$. Of course the K_F values obtained from mono- or biexponential fits are very similar, since in both cases they represent the emission rate at $t = 0$.

From the steady state absorption and delayed fluorescence spectra of benzophenone in CCl_4, Sun et al. [30] obtained $K_F = 1.1 \pm 0.1\ \mu s^{-1}$ by making use of the Birks-Dyson equation [36, 37]. Our K_F value for the isolated molecule can be converted to the corresponding solution quantity by taking into account the refractive index of the solvent, $n = 1.47$ in this spectral range [38]. According to the empty cavity model [39, 40] the fluorescence rates in vacuo and in solution are related by the factor $9n^5(2n^2+1)^{-2}$, so our computed K_F would be converted to about $0.5\ \mu s^{-1}$. Comparing this value with the experimental one, we find it underestimated by about a factor two. Since the $S_0 - S_1$ transition is almost dipole forbidden and presumably very sensitive to the $n \to \pi^*/\pi \to \pi^*$ mixing, both our semiempirical estimate and the application of the Birks-Dyson equation are questionable [36] and further work is planned to investigate this issue.

4 Conclusions

We simulated the photodynamics of benzophenone for the first 20 ps after $n \to \pi^*$ excitation with on the fly trajectory surface hopping calculations. The T_1 state has a mixed $n \to \pi^*/\pi \to \pi^*$ character and therefore shows a sizeable SO coupling with $S_1(n \to \pi^*)$, so that the main ISC channel is found to be due to $S_1 \to T_1$ transitions. In fact we might have slightly underestimated the $S_1 \to T_1$ ISC rate because at non-planar geometries our FOMO-CI T_1 wavefunction shows less $\pi \to \pi^*$ character with respect to the CASSCF one. Nevertheless, our simulations clearly show that T_2 and also higher triplets play a non negligible role in the decay of S_1, because such states are close in energy and more strongly coupled to S_1 than T_1. We obtained a lifetime of S_1 of about 16 ps by a monoexponential fit, or two lifetimes of 6 and 50 ps by a biexponential fit, which seems compatible with experimental determinations [13, 14]. Within the duration of our simulation (20 ps), almost no decay to the ground state takes place, and the most populated triplet is T_1 (about 3/4 of the total). The population of T_2 is around 13% and that of all the higher triplets (mainly T_3 and T_4) about 10%. The nonadiabatic transitions among triplet states are ultrafast, with rate constants ranging from 1 to 50 ps^{-1}. While it would be difficult to unravel experimentally the dynamics within the triplet manifold, the contribution of T_2 and of the higher triplets to differential absorption or

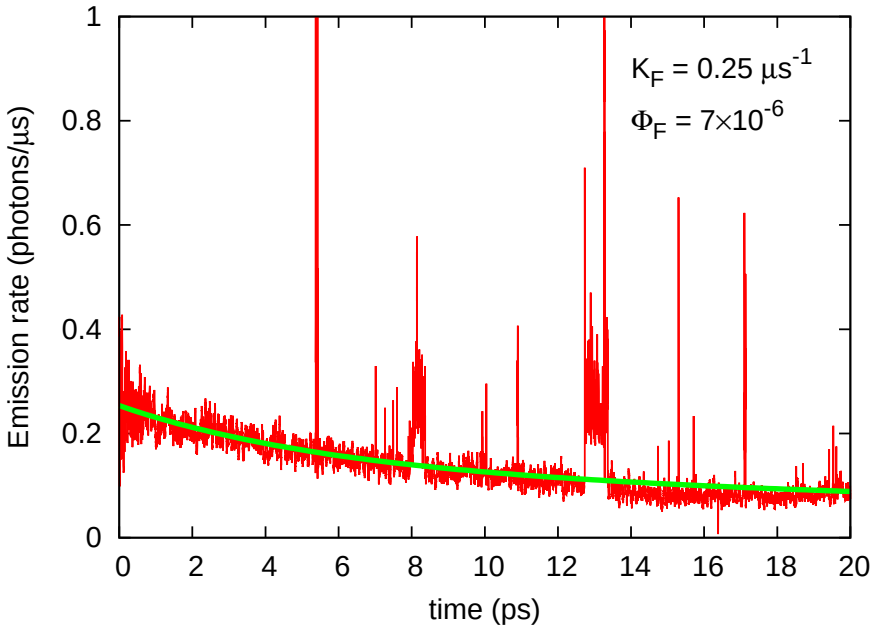

Figure 6: Fluorescence decay. Thin red line: photon emission rate. Thick green line: fit with the biexponential function of eq. 7 see the text. $\Phi_F = K_F[w\tau_1 + (1-w)\tau_2]$ is the fluorescence quantum yield.

photoelectron signals should not be disregarded. We note that vibrational energy loss to the environment may decrease the accessibility of T_2 and of the higher triplets in solution or in other condensed media.

After excitation to S_1, two internal modes start a train of damped oscillations: one is the C=O stretching, with a period of 28 fs, and the other is a combined conrotatory phenyl torsion and phenyl-C-phenyl angle opening, with a period of about 600 fs. An oscillation with about the same frequency was observed by Spighi et al. [14] in time resolved photoelectron spectroscopy experiments and we substantially confirm their attribution to the phenyl torsional motion.

Acknowledgments

This work was supported by grants of the University of Pisa. In particular GG acknowledges the project "Progetti di Ricerca di Ateneo" (grant no. PRA_2015_0038).

References

[1] V. Balzani, P. Ceroni and A. Juris, *Photochemistry and Photophysics*, Wiley-VCH (2014).

[2] R. P. Wayne, *Principles and applications of photochemistry*, Oxford University Press (1988).

[3] M. Consuelo Cuquerella, V. Lhiaubet-Vallet, J. Cadet and M. A. Miranda, *Acc. Chem. Res.*, 2012, **45**, 1558-1570.

[4] E. Dumont, M. Wibowo, D. Roca-Sanjuán, M. Garavelli, X. Assfeld and A. Monari, *J. Phys. Chem. Lett.*, 2015, **6**, 576-580.

[5] R. Kumasaka, A. Kikuchi and M. Yagi, *Photochem. Photobiol.*, 2014, **90**, 727-733.

[6] S. Y. Lee, T. Yasuda, Y. S. Yang, Q. Zhang and C. Adachi, *Angew. Chem. Int. Ed.*, 2014, **53**, 6402-6406.

[7] M. Debije, P. Verbunt, P. Nadkarni, S. Velate, K. Bhaumik, S. Nedumbamana, B. Rowan, B. Richards and T. Hoeks, *Appl. Opt.*, 2011, **50**, 163-169.

[8] T. Itoh, *J. Phys. Chem.*, 1985, **89**, 3949.

[9] B. K. Shah, M. A. J. Rodgers and D. C. Neckers, *J. Phys. Chem. A*, 2004, **108**, 6087-6089.

[10] K. Prater, W. L. Freund and R. M. Bowman, *Chem Phys. Lett.*, 1998, **295**, 82-88.

[11] P. F. McGarry, C. E. Jr. Doubleday, C.-H. Wua, H. A. Staab and N. J. Turro, *J. Photochem. Photobiol. A*, 1994, **77**, 109-117.

[12] H. Miyasaka, K. Morita, K. Kamada and N. Mataga, *Bull. Chem. Soc. Jpn.*, 1990, **63**, 3385-3397.

[13] S. Aloïse, C. Ruckebusch, L. Blanchet, J. Réhault, G. Buntinx and J.-P. Huvenne, *J. Phys. Chem. A*, 2008, **112**, 224-231.

[14] G. Spighi, M.-A. Gaveau, J.-M. Mestdagh, L. Poisson and B. Soep, *Phys. Chem. Chem. Phys.*, 2014, **16**, 9610-9618.

[15] M. Persico and G. Granucci, *Theor. Chem. Acc.*, 2014, **133**, 1526.

[16] G. Granucci, M. Persico and G. Spighi, *J. Chem. Phys.*, 2012, **137**, 22A501.

[17] L. Favero, G. Granucci and M. Persico, *Phys. Chem. Chem. Phys.*, 2013, **15**, 20651.

[18] L. Martínez-Fernández, I. Corral, G. Granucci and M. Persico, *Chem. Sci.*, 2014, **5**, 1336-1347.

[19] T. Cusati, G. Granucci, E. Martínez-Nũnez, F. Martini, M. Persico and S. Vázquez, *J. Phys. Chem. A*, 2012, **116**, 98.

[20] The angle θ is defined as the dihedral formed by the average planes of the two phenyl rings, i.e. the planes obtained by a least squares fit of the positions of their carbon atoms. Assuming pure rotations around the C-C_1 and C-$C_{1'}$ axes by angles $\phi, \phi' \in [0, \pi/2]$ without loss of coplanarity of the phenyl rings and the carbonyl C atom, we have $cos\theta = cos\phi\ cos\phi' + cos\alpha\ sin\phi\ sin\phi'$, where $\alpha = \angle C_1CC_{1'}$. We see that θ is an increasing function of both ϕ and ϕ', so it can be taken as a good descriptor of the loss of planarity of the whole π system.

[21] D.-C. Sergentu, R. Maurice, R. W. A. Havenith, R. Broer and D. Roca-Sanjuán, *Phys. Chem. Chem. Phys.*, 2014, **16**, 25393.

[22] H.-J. Werner, P. J. Knowles, G. Knizia, F. R. Manby and M. Schütz, *WIREs Comput. Mol. Sci.*, 2012, **2**, 242.

[23] G. Granucci and M. Persico, *J. Comput. Chem.*, 2011, **32**, 2690.

[24] M. A. El-Sayed, *J. Chem. Phys.*, 1963, **38**, 2834.

[25] K. W. Holtzlaw and D. W. Pratt, *J. Chem. Phys.*, 1986, **84**, 4713.

[26] N. Ohmori, T. Suzuki and M. Ito, *J. Phys. Chem.*, 1988, **92**, 1086-1093.

[27] V. D. Vachev and J. H. Frederick, *Chem. Phys. Lett.*, 1996, **249**, 476-484.

[28] P. Sett, T. Misra, S. Chattopadhyay, A. K. De and P. K. Mallick, *Vibrational Spectroscopy*, 2007, **44**, 331-342.

[29] W. L. Dilling, *J. Org. Chem.*, 1966, **31**, 1045.

[30] Y.-P. Sun, D. F. Sears and J. Saltiel, *J. Am. Chem. Soc.*, 1989, **111**, 706-711.

[31] G. Bussi and M. Parrinello, *Comp. Phys. Comm.*, 2008, **179**, 26.

[32] G. Granucci, A. Toniolo and M. Persico, *J. Chem. Phys.*, 2001, **114**, 10608.

[33] F. Plasser, G. Granucci, J. Pittner, M. Barbatti, M. Persico and H. Lischka, *J. Chem. Phys.*, 2012, **137**, 22A514.

[34] G. Granucci, M. Persico and A. Zoccante, *J. Chem. Phys.*, 2010, **133**, 134111.

[35] T. Cusati, G. Granucci and M. Persico, *J. Am. Chem. Soc.*, 2011, **133**, 5109-5123.

[36] S. J. Strickler and R. A. Berg, *J. Chem. Phys.*, 1962, **37**, 814.

[37] J. B. Birks and D. J. Dyson, *Proc. R. Soc. A*, 1965, **275**, 135-148.

[38] K. Moutzouris, M. Papamichael, S. C. Betsis, I. Stavrakas, G. Hloupis and D. Triantis, *Appl. Phys. B*, 2013, **116**, 617-622.

[39] R. J. Glauber and M. Lewenstein, *Phys. Rev. A*, 1991, **43**, 467-491.

[40] D. Toptygin, *J. Fluoresc.*, 2003, **13**, 201-219.

Supporting informations

Surface hopping investigation of benzophenone excited state dynamics.

Lucilla Favero, Giovanni Granucci, Maurizio Persico
University of Pisa

Table S1: Target values used in the reparameterization and semiempirical results obtained with the optimized parameters. Energies in eV, distances in Å, angles in degrees, frequencies in cm^{-1}. For the numbering of atoms see the main text.

	target value	semiemp. value	weight
S_0 geom., $\Delta E(S_1 - S_0)$	3.61	3.53	2.5
S_0 geom., $\Delta E(S_2 - S_0)$	4.40	4.56	2.2
S_0 geom., $\Delta E(S_3 - S_0)$	4.40	4.57	2.2
S_0 geom., $\Delta E(S_4 - S_0)$	5.01	4.76	2.5
S_0 geom., $\Delta E(S_5 - S_0)$	5.01	5.05	0.3
S_0 geom., $\Delta E(T_2 - S_0)$	3.61	3.51	1.3
S_0 geom., $\Delta E(S_1 - T_1)$	0.27	0.27	1.3
S_1 geom., $\Delta E(S_1 - S_0)$	2.95	2.93	1.0
S_1 geom., $\Delta E(T_1 - S_0)$	2.78	2.73	1.0
$\Delta E(S_1 - S_0)$, adiabatic	3.25	3.30	1.2
$\Delta E(T_1 - S_0)$, adiabatic	3.00	3.09	1.2
$\Delta E(T_2 - T_1)$, adiabatic	0.25	0.25	0.2
S_0 geom., R(CO)	1.23	1.23	1.2
S_0 geom., R(CC_1)	1.49	1.45	3.8
S_0 geom., angle OCC_1	119.2	119.5	0.7
S_0 geom., dihed. OCC_1C_2	147.0	150.4	0.6
S_0 geom., freq. CO stretch	1682	1738	1.0
S_1 geom., R(CO)	1.32	1.33	0.7
S_1 geom., R(CC_1)	1.45	1.41	2.7
S_1 geom., angle OCC_1	128.1	113.7	0.5
S_1 geom., dihed. OCC_1C_2	156.6	159.2	0.5
T_1 geom., R(CO)	1.33	1.31	0.5
T_1 geom., R(CC_1)	1.44	1.42	2.7
T_1 geom., angle OCC_1	115.5	114.5	0.4
T_1 geom., dihed. OCC_1C_2	153.6	156.9	0.5

Table S2: Optimized semiempirical parameters (AM1 Hamiltonian). The names of the parameters are those used in the MOPAC 2002 documentation [1]. Note that different parameters are used for carbonyl and phenyl C atoms.

	units	C (phenyl)	C (CO)	O	H
U_{ss}	eV	-49.6687239029	-51.5926064181	-89.0096523334	-10.8491535539
U_{pp}	eV	-39.4813823220	-39.1437309074	-77.8379181410	
β_s	eV	-16.1116257628	-15.2814454696	-26.5060604145	-6.3376982810
β_p	eV	-8.3845965271	-7.2293910728	-28.7179596479	
ζ_s	bohr^{-1}	1.6569306913	1.9117163234	3.2500086920	1.2530447780
ζ_p	bohr^{-1}	1.6551097550	1.5066165958	2.5701260986	
α	Å^{-1}	2.7268920403	2.6970289946	4.8641229413	3.0516601405
g_{ss}	eV	12.2719459805	11.7417627149	5.7214695341	12.7862091987
g_{sp}	eV	11.9324870503	11.6321710371	14.7170663247	
g_{pp}	eV	11.3601849803	11.5241312615	14.1552702814	
g_{p2}	eV	10.1373025627	10.0097524401	12.5185353113	
h_{sp}	eV	2.5377929671	2.4791208390	4.1404905520	
K_1		0.0116442026	0.0113409756	0.2805746085	0.1228093162
K_2		0.0459575575	0.0459132653	0.0814799447	0.0050787568
K_3		-0.0200528574	-0.0201275231		-0.0183256794
K_4		-0.0012600880	-0.0012597132		
L_1	Å^{-1}	5.0367158876	4.9870025958	5.0018065393	4.9997012140
L_2	Å^{-1}	5.0074531553	5.0003839163	7.0018495184	5.0013957709
L_3	Å^{-1}	4.9996150387	4.9914903143		2.0001017670
L_4	Å^{-1}	5.0346091244	5.0224265554		
M_1	Å	1.6017218027	1.6010185123	0.8482873880	1.2000291535
M_2	Å	1.8499416727	1.8512004187	1.4205195400	1.7917419639
M_3	Å	2.0513647895	2.0501383394		2.1018835858
M_4	Å	2.6473006889	2.6501071193		

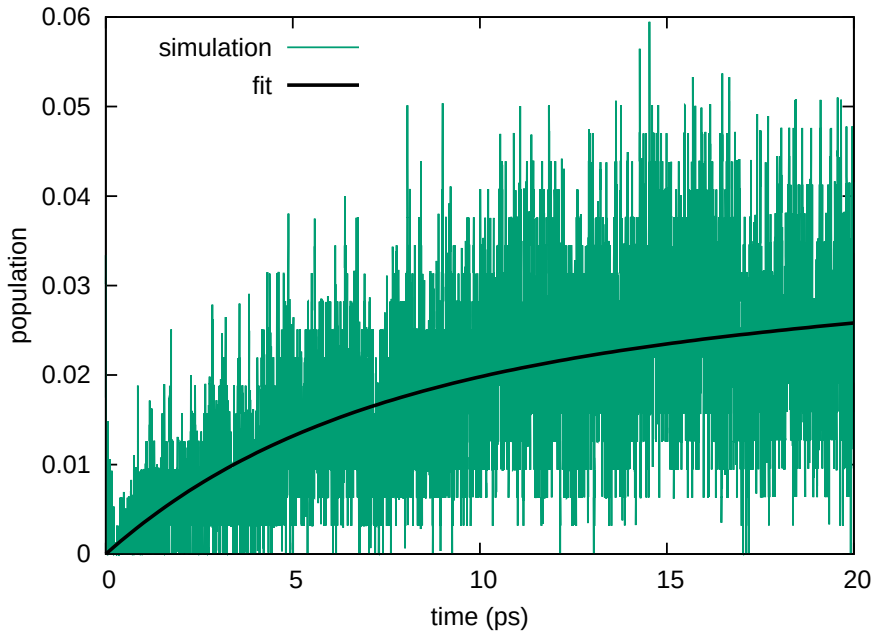

Figure S1: T_3 population. Green curve, simulation; black curve, fit with biexponential decay of S_1.

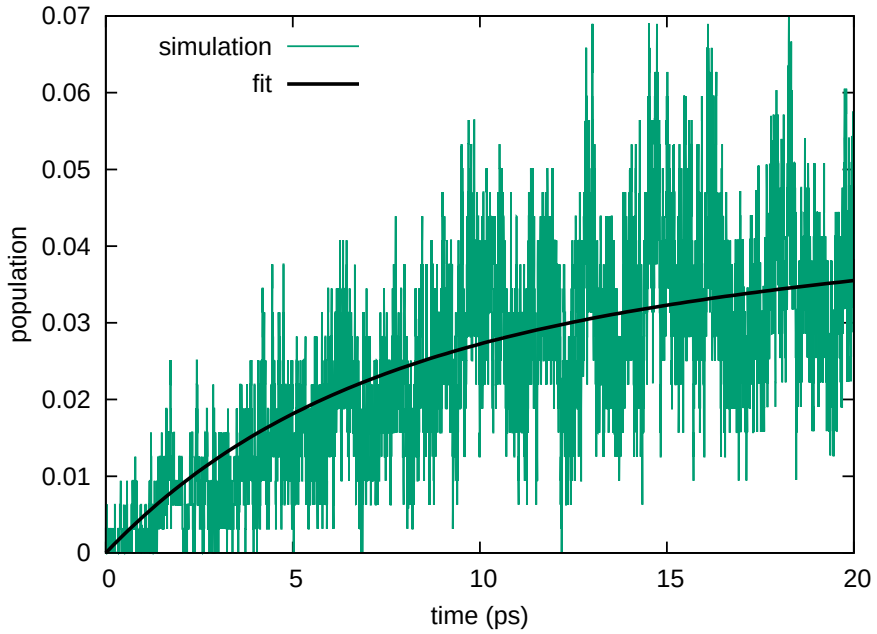

Figure S2: Sum of the populations of T_4 and higher triplets. Green curve, simulation; black curve, fit with biexponential decay of S_1.

Table S3: Radiationless transition rates $\overline{R}_{KL}$ (ps^{-1}) and rate constants $\overline{T}_{KL}$ between spin-diabatic states (or groups of states), averaged over time intervals $[t_1, t_2]$. Some of the rate constants cannot be reliably determined, because in the given time interval very few hops took place, starting from a state with a small population.

state K	state(s) L	t_1, t_2	$\overline{R}_{K\to L}$	$\overline{R}_{L\to K}$	$\Delta\overline{R}_{K\to L}$	$\overline{T}_{K\to L}$	$\overline{T}_{L\to K}$
S_1	T_1	0, 5	0.038	0.005	0.033	0.045	0.051
S_1	T_1	5,10	0.036	0.007	0.029	0.061	0.022
S_1	T_1	10,15	0.027	0.012	0.015	0.058	0.029
S_1	T_1	15,20	0.015	0.014	0.001	0.038	0.030
S_1	T_1	0,20	0.029	0.009	0.019	0.051	0.033
S_1	T_2	0, 5	0.103	0.085	0.019	0.125	1.376
S_1	T_2	5,10	0.080	0.077	0.003	0.136	1.421
S_1	T_2	10,15	0.075	0.073	0.002	0.163	1.034
S_1	T_2	15,20	0.068	0.065	0.003	0.173	0.816
S_1	T_2	0,20	0.082	0.075	0.007	0.149	1.162
S_1	T_3	0, 5	0.004	0.006	-0.002	0.005	—
S_1	T_3	5,10	0.004	0.004	-0.001	0.007	—
S_1	T_3	10,15	0.006	0.007	-0.001	0.014	0.307
S_1	T_3	15,20	0.007	0.006	0.001	0.018	0.227
S_1	T_3	0,20	0.005	0.006	0.000	0.011	0.133
S_1	$T_4 - T_{10}$	0, 5	0.008	0.003	0.005	0.009	—
S_1	$T_4 - T_{10}$	5,10	0.010	0.003	0.007	0.017	—
S_1	$T_4 - T_{10}$	10,15	0.004	0.004	0.000	0.008	—
S_1	$T_4 - T_{10}$	15,20	0.008	0.006	0.002	0.019	—
S_1	$T_4 - T_{10}$	0,20	0.007	0.004	0.003	0.013	—

Table S3 continued.

state K	state(s) L	t_1, t_2	$\overline{R}_{K\to L}$	$\overline{R}_{L\to K}$	$\Delta\overline{R}_{K\to L}$	$\overline{T}_{K\to L}$	$\overline{T}_{L\to K}$
T_1	T_2	0, 5	1.066	1.008	0.059	7.555	25.4
T_1	T_2	5,10	2.567	2.438	0.129	8.165	44.6
T_1	T_2	10,15	3.453	3.271	0.182	8.475	46.1
T_1	T_2	15,20	3.832	3.599	0.233	8.300	44.8
T_1	T_2	0,20	2.730	2.579	0.151	8.124	40.2
T_1	T_3	0, 5	0.225	0.260	-0.034	1.443	—
T_1	T_3	5,10	0.581	0.605	-0.024	1.859	—
T_1	T_3	10,15	0.810	0.853	-0.043	1.985	37.2
T_1	T_3	15,20	0.866	0.937	-0.071	1.876	38.0
T_1	T_3	0,20	0.621	0.664	-0.043	1.791	18.8
T_1	$T_4 - T_{10}$	0, 5	0.162	0.201	-0.039	1.059	—
T_1	$T_4 - T_{10}$	5,10	0.376	0.480	-0.103	1.183	—
T_1	$T_4 - T_{10}$	10,15	0.535	0.670	-0.135	1.313	—
T_1	$T_4 - T_{10}$	15,20	0.540	0.704	-0.164	1.172	—
T_1	$T_4 - T_{10}$	0,20	0.403	0.514	-0.111	1.182	—
T_2	T_3	0, 5	0.191	0.157	0.033	4.997	—
T_2	T_3	5,10	0.445	0.401	0.043	8.185	—
T_2	T_3	10,15	0.634	0.569	0.065	8.934	24.8
T_2	T_3	15,20	0.691	0.590	0.101	8.604	23.9
T_2	T_3	0,20	0.490	0.429	0.061	7.680	12.2
T_2	$T_4 - T_{10}$	0, 5	0.087	0.046	0.040	2.004	—
T_2	$T_4 - T_{10}$	5,10	0.208	0.128	0.080	3.735	—
T_2	$T_4 - T_{10}$	10,15	0.318	0.195	0.123	4.475	—
T_2	$T_4 - T_{10}$	15,20	0.326	0.196	0.130	4.057	—
T_2	$T_4 - T_{10}$	0,20	0.235	0.141	0.093	3.568	—
T_3	$T_4 - T_{10}$	0, 5	0.060	0.063	-0.003	—	—
T_3	$T_4 - T_{10}$	5,10	0.169	0.151	0.018	—	—
T_3	$T_4 - T_{10}$	10,15	0.266	0.247	0.019	11.7	—
T_3	$T_4 - T_{10}$	15,20	0.250	0.218	0.032	10.1	—
T_3	$T_4 - T_{10}$	0,20	0.186	0.170	0.016	5.45	—

References

[1] J. J. P Stewart, *MOPAC 2002*, Fujitsu Limited, Tokio, Japan.